

# Using Glucose-bound $\text{Fe}_3\text{O}_4$ Magnetic Nanoparticles as Photothermal Agents for Targeted Hyperthermia of Cancer Cells

Ching-Yi Wu, Chia-Hua Lin and Yu-Chie Chen\*

Department of Applied Chemistry, National Chiao Tung University, Hsinchu 300, Taiwan

## Abstract

Cancer remains as a top leading cause of death for decades. Thus, efforts have been devoted in exploring effective therapeutic methods of treating patients suffering from the disease. In this study, we proposed a targeted hyperthermia approach that can be used to inhibit the growth of cancer cells by combining functional iron oxide ( $\text{Fe}_3\text{O}_4$ ) magnetic nanoparticles (MNPs) with illumination of near-infrared (NIR) light. Cancer cells express more glucose receptors on their cell membrane than normal cells. Furthermore,  $\text{Fe}_3\text{O}_4$  MNPs are known to possess photothermal features. An aqueous solution containing the generated MNPs ( $1 \mu\text{g} \mu\text{L}^{-1}$ ,  $100 \mu\text{L}$ ) can be heated from  $37^\circ\text{C}$  to over  $50^\circ\text{C}$  under irradiation of a NIR laser (808 nm) within 3 min. We immobilized glucose-6-phosphate on the surface of  $\text{Fe}_3\text{O}_4$  MNPs (Glu- $\text{Fe}_3\text{O}_4$  MNPs) through phosphate-Fe(III) chelation and used the generated glucose functionalized MNPs as probes to target cancer cells, *i.e.*, hepatocellular, breast, and prostate cancer cells, in which different amounts of Glu receptors were expressed in their cell membrane. After irradiating the MNP-target cell conjugates using a NIR laser (808 nm), the growth of cancer cells containing more Glu receptors can be better inhibited than normal cells containing fewer receptors within 1 min. More than 90% of these cancer cells were killed under NIR light irradiation within 3 min. The results showed that the Glu- $\text{Fe}_3\text{O}_4$  MNP-targeted hyperthermia approach can effectively inhibit the growth of cancer cells. On the basis of the targeting capacity of the Glu- $\text{Fe}_3\text{O}_4$  MNPs against cancer cells, the Glu- $\text{Fe}_3\text{O}_4$  MNP probes can be potentially used as universal probes for the photothermal hyperthermia of cancer cells.

**Keywords:**  $\text{Fe}_3\text{O}_4$  magnetic nanoparticles; Photothermal; Cancer cells; Near infrared light; Hyperthermia

## Introduction

Cancer cells are usually more vulnerable to temperature change than normal cells. Thus, photothermal-based hyperthermia is used as a therapeutic for inhibiting cancer cell growth [1-8]. Heat sources are commonly from electromagnetic radiation [2-8]. Near-infrared (NIR) light has the capacity to penetrate deeper into tissues; thus NIR light is used as the light source in photothermal-based hyperthermia. Nanoparticles (NPs) possess tunable optical absorption capability that make them suitable agents and can be combined with electromagnetic radiation to facilitate photothermal therapy. NPs such as gold NPs [9-12], gold nanorods [3-16], and gold nanoshells [17-21] with absorption capacities in the NIR region are reported to be effective photothermal agents to inhibit the growth of cancer cells. Additionally, iron oxide ( $\text{Fe}_3\text{O}_4$ ) magnetic nanoparticles (MNPs) have been lately demonstrated to be effective photothermal agents for inhibiting the cell growth of pathogens [22]. Furthermore, using  $\text{Fe}_3\text{O}_4$  MNPs for photothermal hyperthermia to inhibit the growth of cancer cells has been reported [23-30]. However, most studies focus on using non-targeting based approach [26-30]. One reason that MNPs are not modified to have targeting capacity is the limited choices of probe molecules and consideration of cost. For example, although antibodies have good specificity toward their target species [31-37], antibody-functionalized MNPs are only good for a short period of time because maintaining the good condition of antibodies on MNPs is difficult. The cost of antibodies is also an obstacle in large-scale use. Furthermore, when the identities of target cells are unknown, using antibody-functionalized MNPs as probes is ineffective. Functionalized NPs with broadband affinities toward different types of cancer cells with a low cost are ideal when conducting photothermal hyperthermia.

Glycolytic enzyme and glucose transporter GLUT-1 are known to be overexpressed in the cell membrane of human cancer cells, owing to cancerous tissues and requiring more glucose than normal tissues

[38,39]. The phenomenon was discovered by the German scientist Otto Warburg, and therefore it is so called Warburg effect [40,41]. On the basis of this discovery, we used glucose immobilized NPs as broadband affinity probes toward cancer cells through recognition of the GLUT-1 on the cells.  $\text{Fe}_3\text{O}_4$  MNPs can interact with phosphorylated species by Fe-phosphate chelation [42]. Thus, glucose was immobilized on the MNPs, by linking glucose-6-phosphate and  $\text{Fe}_3\text{O}_4$  MNPs through phosphate-Fe(III) chelation. The generated Glu- $\text{Fe}_3\text{O}_4$  MNPs were used as probes to target cancer cells. The generated Glu- $\text{Fe}_3\text{O}_4$  MNPs have several desirable features including magnetic property, photothermal capability, and targeting ability for cancer cells. The effectiveness of using Glu- $\text{Fe}_3\text{O}_4$  MNPs combined with illumination of NIR light to inhibit the cell growth of target cancer cells was investigated in this study.

## Experimental Section

### Reagents and materials

Iron(III) chloride hexahydrate, sodium bicarbonate, tetramethylammonium hydroxide pentahydrate, kanamycin, D-glucose-6-phosphate dipotassium salt, 4-(2-hydroxyethyl) piperazine-1-ethanesulfonic acid, sodium pyruvate, dimethyl sulfoxide (DMSO), trypan blue solution (0.4%), 3-(4,5-dimethylthiazol-2-

\*Corresponding author: Yu-Chie Chen, Department of Applied Chemistry, National Chiao Tung University, Hsinchu 300, Taiwan, Tel: 886-3-5131527; Fax: 886-3-5723764; E-mail: [yuchie@mail.nctu.edu.tw](mailto:yuchie@mail.nctu.edu.tw)

Received December 12, 2014; Accepted January 23, 2015; Published February 03, 2015

**Citation:** Wu CY, Lin CH, Chen YC (2015) Using Glucose-bound  $\text{Fe}_3\text{O}_4$  Magnetic Nanoparticles as Photothermal Agents for Targeted Hyperthermia of Cancer Cells. J Nanomed Nanotechnol 6: 264. doi:10.4172/2157-7439.1000264

**Copyright:** © 2015 Wu CY, et al. This is an open-access article distributed under the terms of the Creative Commons Attribution License, which permits unrestricted use, distribution, and reproduction in any medium, provided the original author and source are credited.

yl)-3,5-diphenylformazan (MTT formazan, powder) ammonium hydroxide solution (30%–33%), Roswell Park Memorial Institute (RPMI)-1640 medium (with L-glutamine), Dulbecco's modified eagle medium-high glucose (DMEM), and minimum essential medium eagle (MEM) were purchased from Sigma-Aldrich (St. Louis, MO, USA). Mammary epithelium basal medium (MEBM) did not contain antimicrobial agents. Sodium sulfite was purchased from Riedel-de Haën (Seelze, Germany). Hydrochloric acid (36.5–38.0%) and dextrose anhydrous powder were purchased from J. T. Baker (Phillipsburg, NJ, USA). Streptomycin sulfate was purchased from Merck (Darmstadt, Germany). Phosphate buffered saline (PBS) (10× without calcium without magnesium) solution was purchased from Biowest (Nuaille, France). Fetal bovine serum (FBS) and insulin (human recombinant) were obtained from Biological Industries (Kibbutz Beit Haemek, Israel). Hoechst 33342 dye was obtained from Life Technologies (Eugene, OR, USA). Prostate cancer cells (LNCap clone FGC), breast cancer cells (Hs578T and T-47D), and Hep G2 cancer cells were purchased from the Food Industry Research and Development Institute (Hsinchu, Taiwan). Mammary gland/breast cells MCF-10A (CRL-10317™) were purchased from the American Type Culture Collection (Manassas, VA, USA).

### Generation of functional Fe<sub>3</sub>O<sub>4</sub> MNPs

Iron (III) chloride (3.24 g) was dissolved in aqueous HCl (2 M, 6 mL), in a double-necked flask. Deionized water was added into the double-necked flask to have a final volume of 50 mL. The air in the flask was pumped out by a vacuum pump, and was replaced by nitrogen gas. The reaction in the flask was stirred under nitrogen protection followed by injection of sodium sulfite solution (0.08 M, 25 mL), and aqueous ammonia (5%, 22.5 mL) using two syringe pumps with the flow rates of 1.7 and 0.6 mL min<sup>-1</sup>, respectively. The reaction was continuously stirred at 70°C for another 30 min. The generated Fe<sub>3</sub>O<sub>4</sub> MNPs were collected by magnetic isolation, and aggregated by applying an external magnetic field followed by elimination of the supernatant after the reaction solution was cooled to room temperature. The remaining Fe<sub>3</sub>O<sub>4</sub> MNPs were rinsed with deionized water (40 mL×2). The MNPs were then magnetically isolated and the supernatant was removed. Tetramethylammonium hydroxide solution (2.5 mg mL<sup>-1</sup>, 20 mL) was added to Fe<sub>3</sub>O<sub>4</sub> MNP suspension (20 mL) to disperse the MNPs well in the solution under stirring for 1 h. The well dispersed Fe<sub>3</sub>O<sub>4</sub> MNPs were magnetically isolated followed by elimination of the supernatant and rinsed with deionized water (40 mL×2). The Fe<sub>3</sub>O<sub>4</sub> MNPs were re-suspended in deionized water and stored in a refrigerator at 4 °C before use.

The Glu-Fe<sub>3</sub>O<sub>4</sub> MNPs were freshly prepared by vortex-mixing the Fe<sub>3</sub>O<sub>4</sub> MNPs (1 mg) with D-glucose-6-phosphate dipotassium (1 mM, 1 mL) in PBS buffer for 3 h. The excess D-glucose-6-phosphate dipotassium was removed by rinsing with PBS (1 mL×3).

### Characterization of the MNPs

The generated MNPs were 2000-fold and diluted by deionized water before placing the solution (2 µL) on a copper disk with 200 mesh coated with carbon (No. 01800-F, Ted Pella, Inc.). After dried at room temperature, the sample was further dried by using a vacuum pump to remove the remaining solvent. The sample was under investigation using a JEM2000 FX II TEM from JEOL (Tokyo, Japan). The functional groups on the surface of the MNPs were analyzed by a PerkinElmer infrared (IR) spectroscope (Waltham, MA, USA). Prior to IR spectroscopic analysis, the MNPs and KBr powder were placed in an oven at 60°C for 12 h to remove moisture. Subsequently, the MNP

sample and KBr powder were mixed with a weight ratio of 1/100 and milled together to make a tablet under a high pressure of ~4000 psi.

### Observation of microscopic images of the cellular uptake of Glu-Fe<sub>3</sub>O<sub>4</sub> MNPs

Mode cells (40000 cells, 1 mL) were loaded on a glass coverslip in a 6 well plate and cultured at 37°C for one day. After rinse, new medium containing Glu-Fe<sub>3</sub>O<sub>4</sub> MNPs (0.5 mg) were then mixed with the cells followed by incubation for 4 h. The cells were rinsed with PBS buffer (1 mL×3) under shaking for 10 min. The cells were then fixed by addition of 4% formalin (1 mL) and standing at 37°C for 1 h followed by rinse with PBS buffer (1 mL×3) under shaking for 10 min. Block solution (0.1 mL) composed of 10% FBS and 0.25% Triton X-100 prepared in PBS buffer was added to the cell samples and stood at 37°C for 1 h. Hoechst 33342 dye (0.01 mg/mL, 0.1 mL) was added to the cell samples and stood at 37°C for 30 min. The resultant cells were rinsed with wash buffer (1 mL×3), which was composed of 0.25% Triton X-100 in PBS buffer, under shaking for 5 min. The cells were then covered with the other glass slide and sealed with nail polish. The samples were ready for observation by a Nikon Eclipse 80i fluorescent microscope.

### Cell biocompatibility test

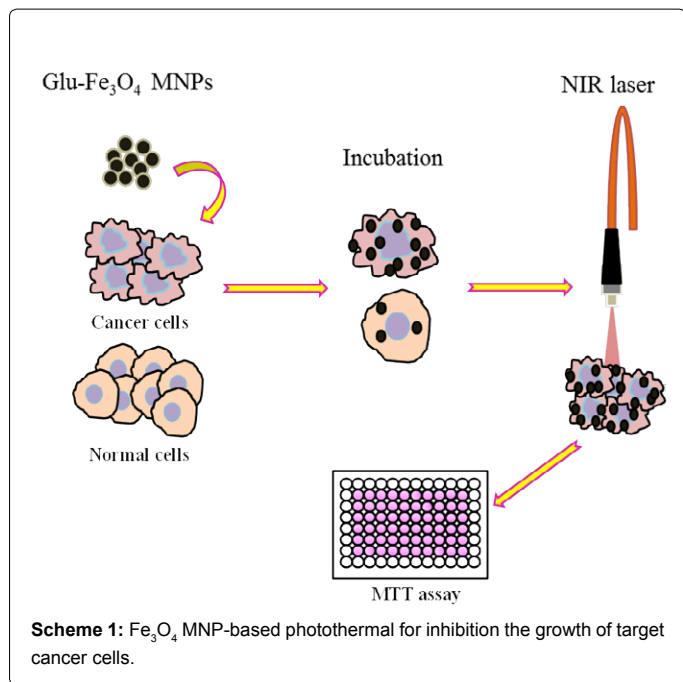
Cell culture was conducted in a Shel Lab CO<sub>2</sub> incubator (5% CO<sub>2</sub>, 37°C) (USA). Cell counting was conducted using a microscope from Hamlat (Amersham, Bucks, UK). Different types of model cells including breast cancer cells (T-47D and Hs578T), mammary gland/breast cells MCF-10A, prostate cancer cells (human LNCaP cone FGC cells), and human hepatocellular carcinoma cells (HePG2 cells) were cultured in different mediums. T-47D and LNCaP clone FGC cells were cultured in RPMI-1640 medium. Hs578T cells were grown in DMEM medium, whereas Hep G2 cells were cultured in MEM medium. MCF-10A cells were incubated in MEBM medium. A given amount of cells (Hs578T ~4000 cells, T-47D ~8000 cells) were incubated with the MNPs at a given concentration for 16 h to examine their cell biocompatibility. MTT can be reduced by the NAD(P)H-dependent cellular oxidoreductase enzymes in metabolically active cells to purple crystal formaza. Thus, the level of the enzymatic product can be used as an indicator for evaluation of cell viability. After the cells were treated with the MNPs, the resultant cells were incubated with MTT (1 mg mL<sup>-1</sup>, 100 µL) for 4 h in a CO<sub>2</sub> incubator (5% CO<sub>2</sub>, 37°C). DMSO (99.9%, 150 µL) was added to dissolve purple formazan. The dissolved purple formazan was analyzed by Varian Cary 50 UV/visible spectroscope (Palo Alto, CA, USA). The difference between the absorbance at the wavelength of 560 nm and the absorbance at the wavelength of 630 nm (as background signal) in the absorption spectrum of the purple formazan sample was recorded to estimate cell viability.

### Examination of the photothermal effects of the functional Fe<sub>3</sub>O<sub>4</sub> MNPs

The functional Fe<sub>3</sub>O<sub>4</sub> MNPs (0-2 mg mL<sup>-1</sup>, 100 µL) rinsed with PBS buffer (1 mL×2) and medium (1 mL×1) were prepared in a 96-well plate. The MNP suspension was irradiated by an NIR laser (808 nm, ~400 mW cm<sup>-2</sup>) for a given time (0-15 min). The fiber output of the NIR laser to the liquid surface on the 96-well plate was distanced at 4.5 cm. The temperature was measured by a thermocouple.

### Photothermal inhibition of the growth of model cells

Scheme 1 shows the photothermal approach for killing target cells. Model cells were prepared in a 96-well plate. Each well was loaded with a given amount of model cells (~4000 cells, 0.1 mL). The cell samples



were incubated at 37°C for 16 h prior to further experiments. After 16 h, the medium was replaced by the medium containing the Glu-Fe<sub>3</sub>O<sub>4</sub> MNPs (1 mg mL<sup>-1</sup>, 100 μL) followed by incubation at 37°C for 12 h. After rinse by fresh medium, the cells were irradiated with an NIR laser for a given time. An NIR laser (λ=808 nm) with an optical fiber (diameter=400 μm) and the maximum power of 1 W was used to examine the photothermal effects of the MNPs. When conducting the experiment, the output current was set to 0.85 A, corresponding to ~400 mW cm<sup>-2</sup>. The distance between the fiber output and the surface of the sample liquid (0–2 mg mL<sup>-1</sup>, 100 μL) placed on a 96 well plate was 4.5 cm.

### Examination of cell survival rate

After photothermal treatment, the survival rates of the cells were examined by the MTT assay. The resultant cells were incubated with MTT (1 mg mL<sup>-1</sup>, 100 μL) for 4 h in an incubator (5% CO<sub>2</sub>) at 37°C. Subsequently, DMSO (99.9%, 150 μL) was added to release the dye. The resultant solution was analyzed by a Varian Cary 50 UV/visible spectrophotometer. The difference between the absorbance at the wavelength of 560 and 630 nm (as background signal) in the absorption spectrum of the sample was recorded for estimation of cell viability.

## Results and Discussion

The Glu-Fe<sub>3</sub>O<sub>4</sub> MNPs were first generated by mixing glucose-6-phosphate with Fe<sub>3</sub>O<sub>4</sub> MNPs. Several analytical methods were used to characterize the generated MNPs. Figures 1A and 1B show the TEM images of Fe<sub>3</sub>O<sub>4</sub> MNPs and Glu-Fe<sub>3</sub>O<sub>4</sub> MNPs, respectively. The average particle size of Fe<sub>3</sub>O<sub>4</sub> MNPs was estimated to be 20 nm. The aggregations of the Glu-Fe<sub>3</sub>O<sub>4</sub> MNPs were quite apparent. The serious aggregations presumably resulted from the hydrogen bonding of glucose units among the Glu-Fe<sub>3</sub>O<sub>4</sub> MNPs. The blurred images may be due to the poor focusing of the high electron energy beam in TEM toward the Fe<sub>3</sub>O<sub>4</sub> MNPs immobilized with glucose. Figures S1A and S1B show the DLS results of the Fe<sub>3</sub>O<sub>4</sub> MNPs and Glu-Fe<sub>3</sub>O<sub>4</sub> MNPs, respectively. It is clear that the size is increased after the surface of Fe<sub>3</sub>O<sub>4</sub> MNPs was coated with glucose. The average size of the MNPs is much larger than

observed from TEM because DLS provides hydrodynamic diameter of the MNPs.

IR spectroscopy was used to characterize the functional groups on the generated MNPs. Figure 2 shows the IR spectra of Fe<sub>3</sub>O<sub>4</sub> MNPs (black), Glu-Fe<sub>3</sub>O<sub>4</sub> MNPs (red), and D-glucose-6-phosphate (blue). In the spectrum of Fe<sub>3</sub>O<sub>4</sub> MNPs, the bands appearing at 493 and 561 cm<sup>-1</sup> correspond to Fe-O vibration modes, while the bands at 889 and 1630 cm<sup>-1</sup> are likely derived from OH-bending [43]. A very evident difference between the IR spectra of the bare Fe<sub>3</sub>O<sub>4</sub> MNPs and the Glu-Fe<sub>3</sub>O<sub>4</sub> MNPs was the broad band appearing at 1100 cm<sup>-1</sup>, which is likely derived from 2° alcohol of the glucose on the Glu-Fe<sub>3</sub>O<sub>4</sub> MNPs [44]. This observation can be taken as the evidence that D-glucose-6-phosphate was successfully bound to the surface of the Fe<sub>3</sub>O<sub>4</sub> MNPs. This band was also clearly observed in the IR spectrum of D-glucose-6-phosphate (blue). Furthermore, the band at 977 cm<sup>-1</sup> presumably representing vibration mode of phosphate in the IR spectrum of D-glucose-6-phosphate disappeared in the IR spectrum of Fe<sub>3</sub>O<sub>4</sub>@glucose MNPs [45], indicating the phosphate group was used in the binding between the glucose and the MNPs.

The photothermal effect of the generated Fe<sub>3</sub>O<sub>4</sub> MNPs was examined. The model cells used in this study were either prepared in DMEM or RPMI. The photothermal effects of the functional MNPs were initially examined in different mediums. Figures 3A and 3B show the plots of the temperature increase (ΔT) versus the irradiation time of an NIR laser obtained from DMEM and RPMI medium containing Fe<sub>3</sub>O<sub>4</sub> MNPs, respectively. The initial temperature was maintained at 37°C. The curve in black was the blank control obtained in the absence of the Fe<sub>3</sub>O<sub>4</sub> MNPs. The temperature of the control sample was increased only 2°C after 15 min. However, the temperature

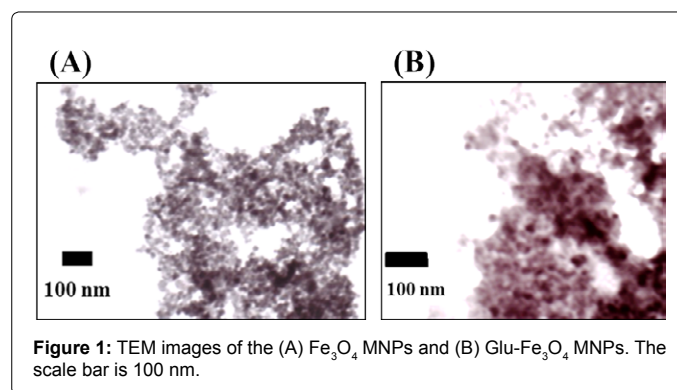


Figure 1: TEM images of the (A) Fe<sub>3</sub>O<sub>4</sub> MNPs and (B) Glu-Fe<sub>3</sub>O<sub>4</sub> MNPs. The scale bar is 100 nm.

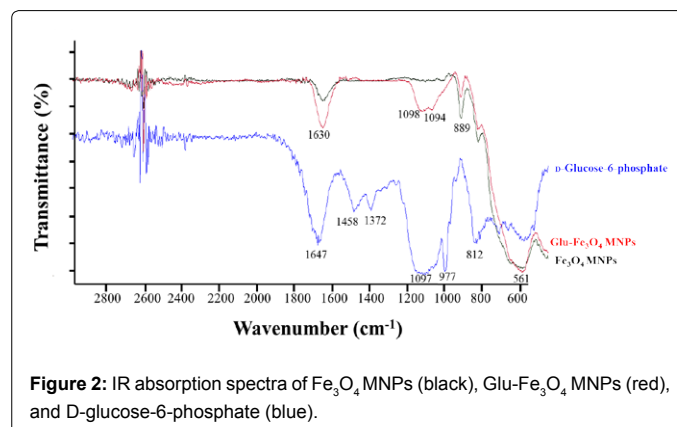
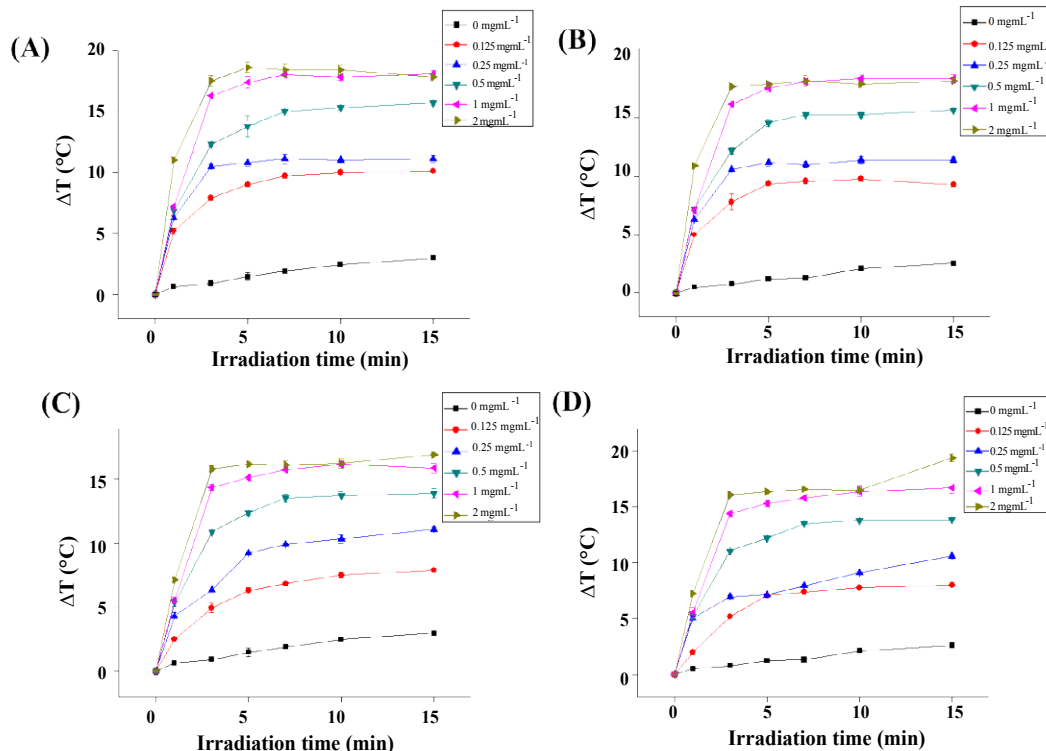


Figure 2: IR absorption spectra of Fe<sub>3</sub>O<sub>4</sub> MNPs (black), Glu-Fe<sub>3</sub>O<sub>4</sub> MNPs (red), and D-glucose-6-phosphate (blue).



**Figure 3:** Plots of the temperature increase ( $\Delta T$ ) versus the irradiation time of an NIR laser obtained from (A) DMEM (0.1 mL) and (B) RPMI medium (0.1 mL) containing different concentrations of Fe<sub>3</sub>O<sub>4</sub> MNPs and from (C) DMEM (0.1 mL) and (D) RPMI medium (0.1 mL) containing different concentrations of Glu-Fe<sub>3</sub>O<sub>4</sub> MNPs. The temperature of the samples was maintained at 37°C in the beginning of the laser irradiation.

increase was proportional to the irradiation time of the NIR light in the presence of the Fe<sub>3</sub>O<sub>4</sub> MNPs. Within 3 min, all the suspensions reached their maximum temperature owing to the equilibrium with ambient temperature. The maximum temperature was higher in the suspension containing higher concentrations of the Fe<sub>3</sub>O<sub>4</sub> MNPs. Furthermore, the temperature was elevated significantly as the concentration of the Fe<sub>3</sub>O<sub>4</sub> MNPs was increased. Within 3 min, the temperature ( $\Delta T$ ) of the suspension (2 mg mL<sup>-1</sup>, 100  $\mu$ L) was increased  $\sim$ 18°C. The temperature was increased from 37°C to 55°C. The photothermal effects of the Fe<sub>3</sub>O<sub>4</sub> MNPs prepared in different mediums were similar. Furthermore, the maximum temperature reached  $\sim$ 55°C when the concentration of the MNPs in the suspension was  $\geq$  1 mg mL<sup>-1</sup>. Figures 3C and 3D show the plots obtained by irradiating the mediums containing different concentrations of the Glu-Fe<sub>3</sub>O<sub>4</sub> MNPs as a function of time with the illumination of the NIR laser (808 nm,  $\sim$ 400 mW cm<sup>-2</sup>). Similar effects were observed as those shown in Figures 3A and 3B. Nevertheless, the maximum  $\Delta T$  was  $\sim$ 16°C, slightly lower than that observed in Figures 3A and 3B. This is taking into consideration the weight contribution of glucose to the Glu-Fe<sub>3</sub>O<sub>4</sub> MNPs. Glucose does not have photothermal effects but it contributes to the total weight of the suspension. Although the photothermal efficiency of the Glu-Fe<sub>3</sub>O<sub>4</sub> MNPs was slightly worse, the temperature of the samples containing Glu-Fe<sub>3</sub>O<sub>4</sub> MNPs under NIR light irradiation was quickly raised and reached to the maximum equilibrium temperature within 3 min. The results showed that the Fe<sub>3</sub>O<sub>4</sub> MNPs and Glu-Fe<sub>3</sub>O<sub>4</sub> have desirable photothermal effect.

After demonstrating the photothermal effects of the generated MNPs, the cytotoxicity test was conducted. MTT Assay was conducted to examine the cell biocompatibility of the MNPs after incubating

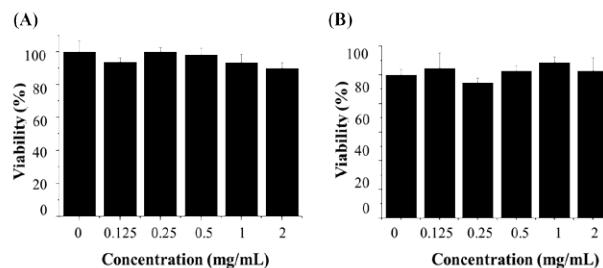
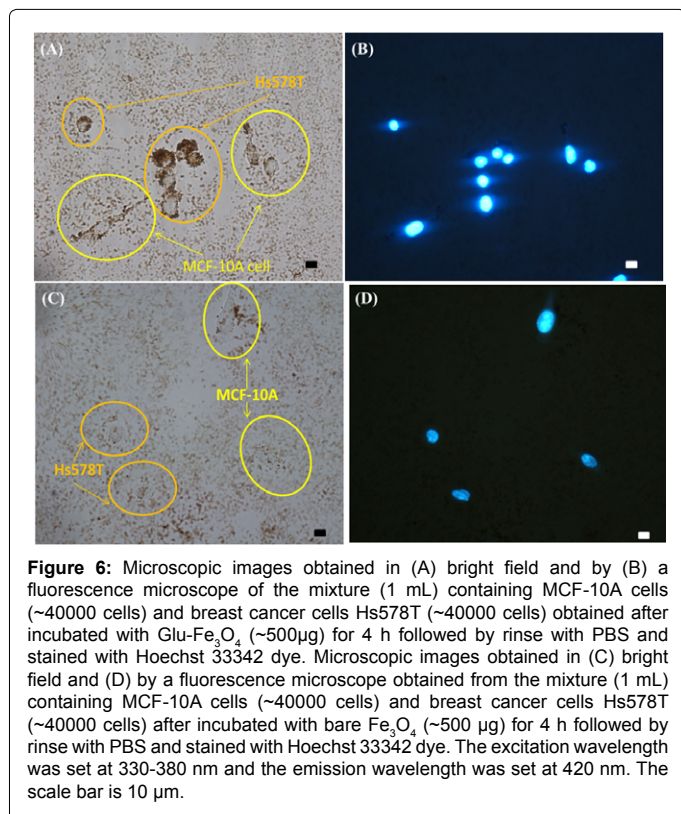
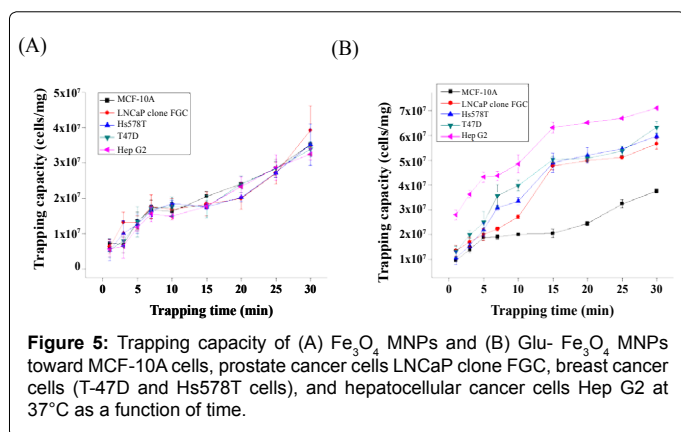


**Figure 4:** Examination of cell biocompatibility of the Glu-Fe<sub>3</sub>O<sub>4</sub> MNPs. Cell viability test obtained by incubating Glu-Fe<sub>3</sub>O<sub>4</sub> MNPs at different concentrations with (A) T47D cells ( $\sim$  8000 cells, 0.1 mL) and (B) Hs578T cells ( $\sim$  4000 cells, 0.1 mL).

the MNPs with the model cells including breast cancer cells (T-47D and Hs578T) for 16 h. Figures 4A and 4B show the results of the cell viability test of the Glu-Fe<sub>3</sub>O<sub>4</sub> MNPs incubated with breast cancer cells T-47D and Hs578T, respectively. Clearly, the survival rate was  $>$  90% even with increasing concentration of the MNPs to 2 mg mL<sup>-1</sup> in these two cell samples. The results indicated that these MNPs have good cell biocompatibility.

As mentioned earlier, cancer cells usually overexpress more glucose receptors than normal cells [39]. Consequently, the Glu-Fe<sub>3</sub>O<sub>4</sub> MNPs should have better trapping capacity toward cancer cells than normal cells. According to a previous study [39], hepatocellular carcinoma cells overexpress more glucose receptors than breast cancer cells. The

Glu-Fe<sub>3</sub>O<sub>4</sub> MNPs should have higher affinity toward hepatocellular carcinoma cells than toward breast cancer cells. On the other hand, bare Fe<sub>3</sub>O<sub>4</sub> MNPs should have no preference in trapping different types of cells. Figure 5 shows the trapping capacity of the Fe<sub>3</sub>O<sub>4</sub> MNPs and the Glu-Fe<sub>3</sub>O<sub>4</sub> MNPs toward mammary gland/breast cells MCF-10A, prostate cancer cells LNCaP clone FGC, breast cancer cells (Hs578T and cells T-47D), and hepatocellular cancer cells Hep G2 at 37°C as a function of time. The results indicated that Fe<sub>3</sub>O<sub>4</sub> MNPs had no selectivity toward these cells and its trapping capacities were similar. However, the Glu-Fe<sub>3</sub>O<sub>4</sub> MNPs have better trapping capacity toward hepatocellular cancer cells Hep G2 and worse trapping capacity toward mammary gland/breast cells MCF-10A. Notably, the trapping capacity achieved nearly equilibrium at ~15 min. With prolonged incubation time, the trapping capacity was still increased (Figures 5A and 5B). This was because once cells were trapped on the MNPs, the interactions between cells and cells also took place. Therefore, as the incubation



time was extended, more cells can attach to the cells on the MNPs. Nevertheless, the results showed that the Glu-Fe<sub>3</sub>O<sub>4</sub> MNPs have better trapping capacity toward cancer cells than normal cells. The trapping capacity toward cancer cells is varied, depending on the type of cancer cells containing different numbers of GLUT-1 receptors.

In addition, cancer cells are assumed to have capability to engulf more Glu-Fe<sub>3</sub>O<sub>4</sub> MNPs than normal cells. We observed the optical images obtained after incubating the cell mixture containing cancer cells and normal cell with the Glu-Fe<sub>3</sub>O<sub>4</sub> MNPs to examine the MNP uptake results. Figure 6 shows the microscopic images obtained after incubating the Glu-Fe<sub>3</sub>O<sub>4</sub> MNPs and a cell mixture containing breast cancer cells Hs578T (~40000 cells) and MCF-10A (~40000 cells) for 4 h followed by removing excess MNPs. To investigate the cells clearly, the nuclei of the cells were stained with Hoechst 33342 dye. The cell shape of the breast cancer cells Hs578T is round, whereas MCF-10A cells is spindle shaped. Figures 6A and 6B show the resultant microscope images obtained under bright filed and a fluorescence microscope, respectively. The Glu-Fe<sub>3</sub>O<sub>4</sub> MNPs have brown color. The distribution of the MNPs is clearly seen in the images (Figure 6A). The stained nuclei with blue emission were clearly observed under a fluorescence microscope (Figure 6B). The cytoplasm in round shape cells, i.e. breast cancer cells Hs578T (circled by orange) were distributed with more Glu-Fe<sub>3</sub>O<sub>4</sub> MNPs than that in spindle shaped cells, i.e. MCF-10A cells (circled by yellow). The results correspond to what was expected, cancer cells Hs578T are able to engulf more Glu-Fe<sub>3</sub>O<sub>4</sub> MNPs than MCF-10A cells because cancer cells overexpress more glucose receptors. We also incubated bare Fe<sub>3</sub>O<sub>4</sub> MNPs with the cell mixture. Figures 6C and 6D show the corresponding microscopic images obtained in bright field and by a fluorescence microscope. After the cell mixture was incubated with bare Fe<sub>3</sub>O<sub>4</sub> MNPs for 4 h, the uptake amount of the bare Fe<sub>3</sub>O<sub>4</sub> MNPs by Hs578T cells (circled by orange) was much lower (Figure 6C) than that shown in Figure 6A. Furthermore, the MCF-10A cells seemed internalizing fewer bare Fe<sub>3</sub>O<sub>4</sub> MNPs. The results indicated that the Glu-Fe<sub>3</sub>O<sub>4</sub> MNPs have good affinity toward cancer cells and can facilitate the uptake process.

Photothermal killing experiments were further conducted after demonstrating cancer cells have better MNP engulfment capacity. First, the incubation time and different ratios of MNPs to the model cells were examined. A 96-well plate was loaded with model cells and maintained at the temperature of 37°C. Figure 7 shows the plot obtained by incubating the Glu-Fe<sub>3</sub>O<sub>4</sub> MNPs with model cells followed by irradiating with the NIR light (808 nm, ~400 mW cm<sup>-2</sup>) as a function of time. The results show the highest cell viability observed in incubating MCF-10A cells with the MNPs. The result corresponded to what was obtained in Figure 6, since MCF-10A cells engulfed fewer MNPs than cancer cells. Therefore, MCF-10A cells encountered less photothermal effects than other model cancer cells within a short period of light illumination. The survival rate of the MCF-10 A cells was still ~>95% after being irradiated by the NIR light for 1 min. On the other hand, the cell viability of hepatocellular cancer cells Hep G2 was only ~30% after illumination by the NIR light for 1 min. The cell viability of breast cancer cells (T-47D and Hs578T) was slightly higher, whereas prostate cancer cells LNCaP clone FGC was even higher. As mentioned earlier, the number of glucose receptors on the cell membrane is in the order of hepatocellular cancer cells > breast cancer cells> prostate cancer cells > normal cells [39]. For cells that can overexpress more glucose receptors on the cell membrane, the cell survival rate is lower. The photothermal killing effect is more apparent for those cancer cells that can overexpress more GLUT 1 receptors. As the illumination time was longer than 1 min, MCF-10A cells were damaged more. Nevertheless,

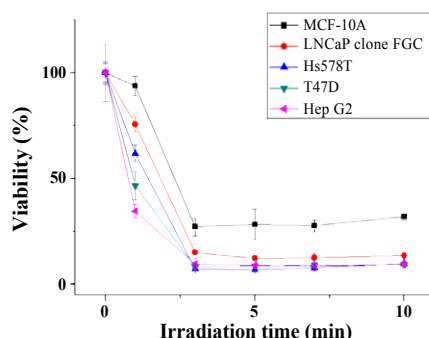


**Figure 7:** Examination of cell survival rate of different model cells using the current Glu-Fe<sub>3</sub>O<sub>4</sub> targeted photothermal hyperthermia approach. The model cells (~4000 cells, 0.1 mL) mammary gland/breast cells MCF-10A, prostate cancer cells LNCaP clone FGC, breast cancer cells (Hs578T and T-47D), and hepatocellular cancer cells Hep G2 were incubated individually with the Glu-Fe<sub>3</sub>O<sub>4</sub> MNPs (0.1 g) (0.1 mL, 1 mg mL<sup>-1</sup>) at 37°C for 12 h followed by rinse with medium. The original concentration of the Glu-Fe<sub>3</sub>O<sub>4</sub> was. The resultant cells were irradiated with an NIR laser (808 nm) for different times. MTT assays were performed to estimate the cell survival rate. Three replicated were conducted.

the illumination time can be controlled to be within 1 min to limit the damage on normal cells. Furthermore, the illumination can be applied in multiple times with a short period of time (< 1 min) to reduce the damage on normal cells.

## Conclusions

The study demonstrated that Glu-Fe<sub>3</sub>O<sub>4</sub> MNPs can be used as universal targeting probes and photothermal agents for several cancer cells. Compare with conventional functional probes, the functional NPs are more cost-effective. Furthermore, the cell toxicity of the Glu-Fe<sub>3</sub>O<sub>4</sub> MNPs was low. Our results show that the Glu-Fe<sub>3</sub>O<sub>4</sub> MNPs have higher targeting capacity toward cancer cells than normal cells. On the basis of our results, cancer cells can engulf more Glu-Fe<sub>3</sub>O<sub>4</sub> MNPs than normal cells. Cancer cells were damaged more when using this MNP-based photothermal hyperemia approach. The photokilling efficiency for cancer cells was quite high. Within 1 min, only ~30% hepatocellular cancer cells HepG2 treated with the Glu-Fe<sub>3</sub>O<sub>4</sub> MNPs and illuminated by the NIR light for 1 min survived, while only ~10% normal cells were damaged. These results suggest the potential to be used in the treatment of cancer patients. Further *in vivo* studies should be conducted to demonstrate its practical use of the current approach.

## Acknowledgement

We thank the Ministry of Science and Technology of Taiwan (NSC 102-2113-M-009-019-MY3) for the support of this work financially.

## References

1. van der Zee J (2003) Heating the patient: a promising approach? *Ann Oncol* 13: 1173-1184.
2. Hergt R, Dutz S, Müller R, Zeisberger M (2006) Magnetic particle hyperthermia: nanoparticle magnetism and materials development for cancer therapy. *J Phys Condens Matter* 18: S2919-S2934.
3. Fortin JP, Wilhelm C, Servais J, Menager C, Bacri JC, et al. (2007) Size-sorted anionic iron oxide nanomagnets as colloidal mediators for magnetic hyperthermia. *J Am Chem Soc* 129: 2628-2635.
4. Creixell M, Bohórquez AC, Torres-Lugo M, Rinaldi C (2001) EGFR-targeted magnetic nanoparticle heaters kill cancer cells without a perceptible temperature rise. *ACS Nano* 5: 7124-7129.

5. Schmidt AM (2005) Induction heating of novel thermoresponsive ferrofluids. *J Magn Magn Mater* 289: 5-8.
6. Alphanbéry E, Faure S, Seksek O, Guyot F, Chebbi I (2011) Chains of magnetosomes extracted from AMB-1 magnetotactic bacteria for application in alternative magnetic field cancer therapy. *ACS Nano* 5: 6279-6296.
7. Chen Y, Bose A, Bothun GD (2010) Controlled release from bilayer-decorated magnetoliposomes via electromagnetic heating. *ACS Nano* 4: 3215-3221.
8. Bae KH, Park M, Do MJ, Lee N, Ryu JH, et al. (2012) Chitosan oligosaccharide-stabilized ferrimagnetic iron oxide nanocubes for magnetically modulated cancer hyperthermia. *ACS Nano* 6: 5266-5273.
9. Van de Broek B, Devoogdt N, D'Hollander A, Gijs HL, Jans K, et al. (2011) Specific cell targeting with nanobody conjugated branched gold nanoparticles for photothermal therapy. *ACS Nano* 5: 4319-4328.
10. Huang X, Jain PK, El-Sayed IH, El-Sayed MA (2008) Plasmonic photothermal therapy (PPTT) using gold nanoparticles. *Lasers Med Sci* 23: 217-228.
11. Kennedy LC, Bickford LR, Lewinski NA, Coughlin AJ, et al. (2011) A new era for cancer treatment: gold-nanoparticle-mediated thermal therapies. *Small* 7: 169-183.
12. Gobin AM, Watkins EM, Quevedo E, Colvin VL, West JL (2010) Near-infrared-resonant gold/gold sulfide nanoparticles as a photothermal cancer therapeutic agent. *Small* 6: 745-752.
13. Dickerson EB, Dreaden EC, Huang X, El-Sayed IH, Chu H, et al. (2008) Gold nanorod assisted near-infrared plasmonic photothermal therapy (PPTT) of squamous cell carcinoma in mice. *Cancer Lett* 269: 57-66.
14. Huang X, El-Sayed IH, Qian W, El-Sayed MA (2006) Cancer cell imaging and photothermal therapy in the near-infrared region by using gold nanorods. *J Am Chem Soc* 128: 2115-2120.
15. Goodrich GP, Bao L, Gill-Sharp K, Sang KL, Wang J, et al. (2010) Photothermal therapy in a murine colon cancer model using near-infrared absorbing gold nanorods. *J Biomed Opt* 15: 018001.
16. Choi WI, Sahu A, Kim YH, Tae G (2012) Photothermal cancer therapy and imaging based on gold nanorods. *Ann Biomed Eng* 40: 534-546.
17. Vankayala R, Lin CC, Kalluru P, Chiang CS, Hwang KC (2014) Gold nanoshells-mediated bimodal photodynamic and photothermal cancer treatment using ultra-low doses of near infra-red light. *Biomaterials* 35: 5527-5538.
18. Melancon MP, Lu W, Yang Z, Zhang R, Cheng Z, et al. (2008) In vitro and in vivo targeting of hollow gold nanoshells directed at epidermal growth factor receptor for photothermal ablation therapy. *Mol Cancer Ther* 7: 1730-1739.
19. Hirsch LR, Stafford RJ, Bankson JA, Sershen SR, Rivera B, et al. (2003) Nanoshell-mediated near-infrared thermal therapy of tumors under magnetic resonance guidance. *Proc Natl Acad Sci USA* 100: 13549-13554.
20. O'Neal DP, Hirsch LR, Halas NJ, Payne JD, West JL (2004) Photo-thermal tumor ablation in mice using near infrared-absorbing nanoparticles. *Cancer Lett* 209: 171-176.
21. Ayala-Orozco C, Urban C, Knight MW, Urban AS, Neumann O, et al. (2014) Au nanomatryoshkas as efficient near-Infrared photothermal transducers for cancer treatment: benchmarking against nanoshells. *ACS Nano* 24: 6372-6381.
22. Yu TJ, Li PH, Tseng TW, Chen YC (2011) Multifunctional Fe<sub>3</sub>O<sub>4</sub>/alumina core/shell MNPs as photothermal agents for targeted hyperthermia of nosocomial and antibiotic-resistant bacteria. *Nanomedicine* 6:1353-1363.
23. Liao MY, Lai PS, Yu HP, Lin HP, Huang CC (2012) Innovative ligand-assisted synthesis of NIR-activated iron oxide for cancer theranostics. *Chem Commun* 48: 5319-5321.
24. Huang HS, Hainfeld JF (2013) Intravenous magnetic nanoparticle cancer hyperthermia. *Int J Nanomedicine* 8: 2521-3252.
25. Chu M, Shao Y, Peng J, Dai X, Li H, et al. (2013) Near-infrared laser light mediated cancer therapy by photothermal effect of Fe<sub>3</sub>O<sub>4</sub> magnetic nanoparticles. *Biomaterials* 34: 4078-4088.
26. DeVita V T Jr, Chu E (2008) A history of cancer chemotherapy. *Cancer Res* 68: 8643-8653.
27. Muthana M, Scott SD, Farrow N, Morrow F, Murdoch C, et al. (2008) A novel magnetic approach to enhance the efficacy of cell-based gene therapies. *Gene Ther* 15: 902-910.

28. Rich JN, Bao S (2007) Chemotherapy and cancer stem cells. *Cell Stem Cell* 1: 353-355.
29. Pardoll D, Drake C (2012) Immunotherapy earns its spot in the ranks of cancer therapy. *J Exp Med* 209: 201-209.
30. Shen S, Wang S, Zheng R, Zhu X, Jiang X, et al. (2015) Magnetic nanoparticle clusters for photothermal therapy with near-infrared irradiation? *Biomater* 39: 67-74.
31. Maloney EK, McLaughlin J, Dagdigian NE, Garrett LM, Connors KM, et al. (2003) An anti-insulin-like growth factor I receptor antibody that is a potent inhibitor of cancer cell proliferation. *Cancer Res* 63: 5073-5083.
32. Kwok HF (2013) Antibody research targeting Cathepsin S for cancer therapy. *Adv Biosci Biotechnol* 4: 17-20.
33. Pichinuk E, Benhar I, Jacobi O, Chalik M, Weiss L, et al. (2012) Antibody targeting of cell-bound MUC1 SEA domain kills tumor cells. *Cancer Res* 72: 3324-3336.
34. Feridani AH, Holmqvist B, Sjogren HO, Strand SE, Tennvall J, et al. (2007) Combined flow cytometry and confocal laser scanning microscopy for evaluation of BR96 antibody cancer cell targeting and internalization. *Cytometry A* 71: 361-370.
35. Carter P (2001) Improving the efficacy of antibody-based cancer therapies. *Nat Rev Cancer* 1: 118-129.
36. Adams GP, Weiner LM (2005) Monoclonal antibody therapy of cancer. *Nat Biotechnol* 23: 1147-1157.
37. Zdobnova TA, Stremovskiy OA, Lebedenko EN, Deyev SM (2012) Self-assembling complexes of quantum dots and scFv antibodies for cancer cell targeting and imaging. *PLoS One* 7: e48248.
38. Fuster MM, Esko JD (2005) The sweet and sour of cancer: glycans as novel therapeutic targets. *Nat Rev Cancer* 5: 526-542.
39. Calvaresi EC, Hergenrother PJ (2013) Glucose conjugation for the specific targeting and treatment of cancer. *Chem Sci* 4: 2319-2333.
40. Warburg O, Wind F, Negelein E (1927) The metabolism of tumors in the body. *J Gen Physiol* 8: 519-530.
41. Warburg O (1956) On the origin of cancer cells. *Science* 123: 309-314.
42. Butkus MA, Grasso D, Schulthess CP, Wijnja H (1998) Surface complexation modeling of phosphate adsorption by water treatment residual. *J Environ Qual* 27: 1055-1063.
43. Cornell RM, Schwertmann U (2006) The iron oxides: structure, properties, reactions, occurrences and uses.
44. Hashimoto A, Kameoka T (2008) Applications of infrared spectroscopy to biochemical, food and agricultural process. *Appl Spectrosc Rev* 43: 416-451.
45. Nakanishi K, Hashimoto A, Pan T, Kanou M, Kameoka T (2003) Mid-infrared spectroscopic measurement of ionic dissociative materials in the metabolic pathway. *Appl Spectrosc* 57: 1510-1516.